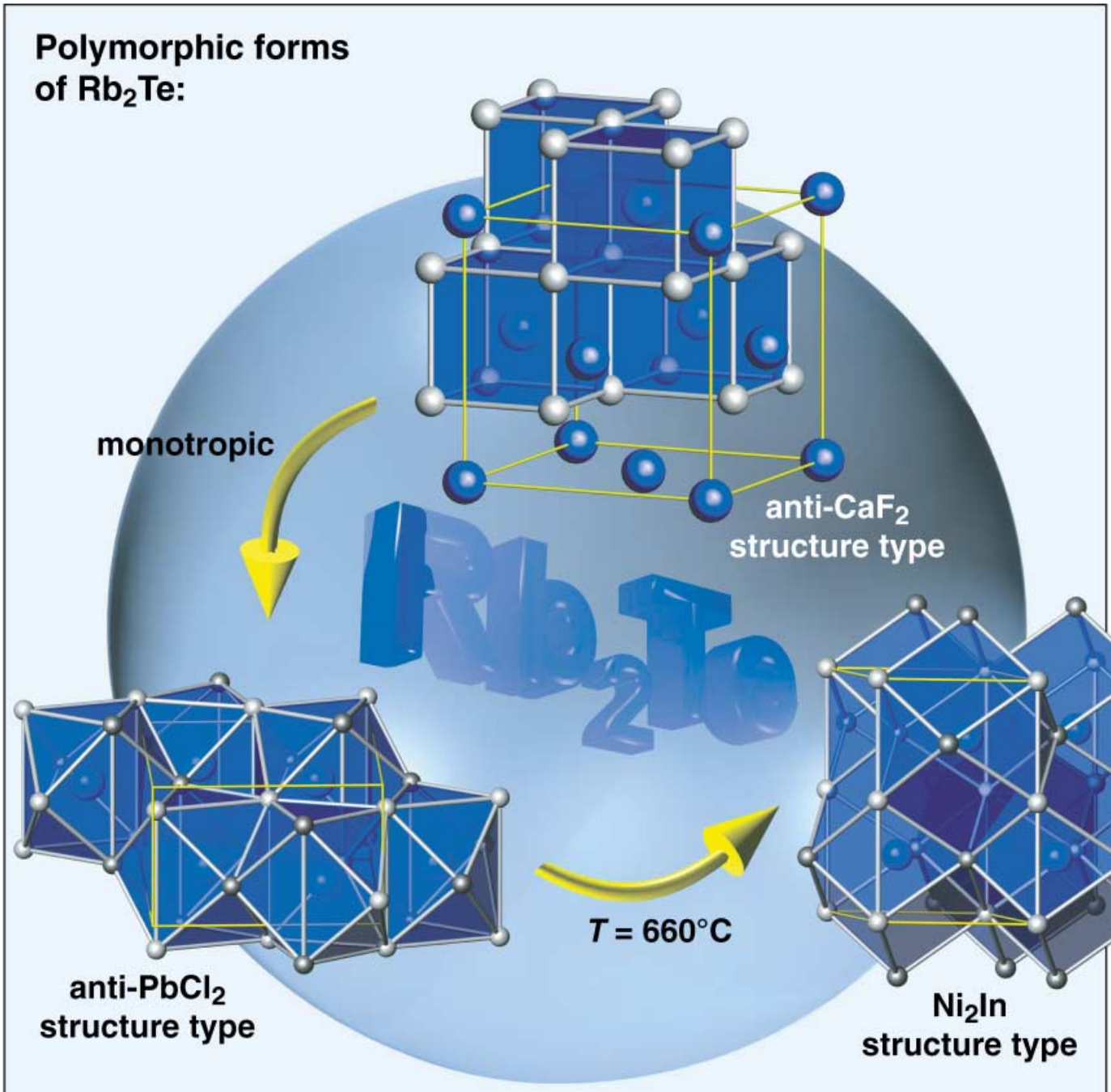

The polymorphic form of Rb_2Te that is metastable at room temperature crystallizes in the anti-CaF_2 structure type. Upon warming, it converts irreversibly into the anti-$PbCl_2$ type. Above $T = 660\,^{\circ}C$, Rb_2Te adopts a Ni_2In-type structure.

In the given polymorph series, the coordination number of the Te atom increases from 8 (cubic), through 9 (double-capped trigonal prism), to 11 (Edshammar polyhedra), which is uncharacteristic of a high-temperature polymorph series.

For more information, see the following pages.

  1433-7851/02/4115-2725 $ 20.00+.50/0

Polymorphic Forms of Rubidium Telluride Rb_2Te**

Klaus Stöwe* and Stephan Appel

The crystal structures of the di(alkali-metal) monochalcogenides A_2Q are known for all the compounds with A = Li–Cs and Q = O–Te, except for one. All the structurally characterized compounds, except the cesium chalcogenides, crystallize in a fluorite-type structure[1–4] under normal conditions, whereas the cesium chalcogenides, except Cs_2O, which can be assigned to the anti-$CdCl_2$ type,[5] crystallize in an anti-$PbCl_2$-type structure.[4, 6] The exception mentioned above is the compound Rb_2Te, whose structure has not yet been reported in the literature. On the basis of poor data, complicated diagrams were obtained from diffraction experiments, but they could not be indexed.[7] This is as a result of the difficulties in the synthesis and the instability of the substance.[4] Within the scope of our investigations into ternary alkali rare-earth tellurides, we also intended to use the compound Rb_2Te as a flux during synthesis. We therefore considered a characterization of Rb_2Te as a necessary prerequisite.

We developed special laboratory glassware for the synthesis of the highly unstable Rb_2Te.[8] The apparatus allows the single-phase preparation of all alkali chalcogenides. During synthesis of Rb_2Te from its elements in liquid ammonia, the product was formed as a yellow-green powder after extraction of the excess rubidium metal. A light-yellow product is obtained after prolonged extraction with ammonia. The ammonia solution above the product is light-blue in color during the whole extraction process as a result of the dissolved rubidium metal. From this observation, together with the occurrence of Bragg peaks in the powder diffraction pattern that indicate foreign phases, we deduced that the light-yellow product has a lower Rb content than the yellow-green substance. The phase composition of the products was analyzed by means of X-ray powder diffraction, and their thermal stability was determined by means of differential thermal analysis (DTA).

DTA of the yellow-green thermally untreated product obtained from liquid ammonia (i.e. the stoichiometric compound) shows several phase transitions (Figure 1): above 200 °C it slowly undergoes an irreversible transformation, which ends at about 470 °C (heating rate of 5 °C min^{-1}). The irreversibility of the phase transition can be concluded from the cooling curve: the exothermic effect of the heating curve in the temperature range below 500 °C is no longer observed. Furthermore, this effect is also not observed when the sample is reheated, and even samples that have been annealed for several days at 200 °C do not undergo a retransformation.

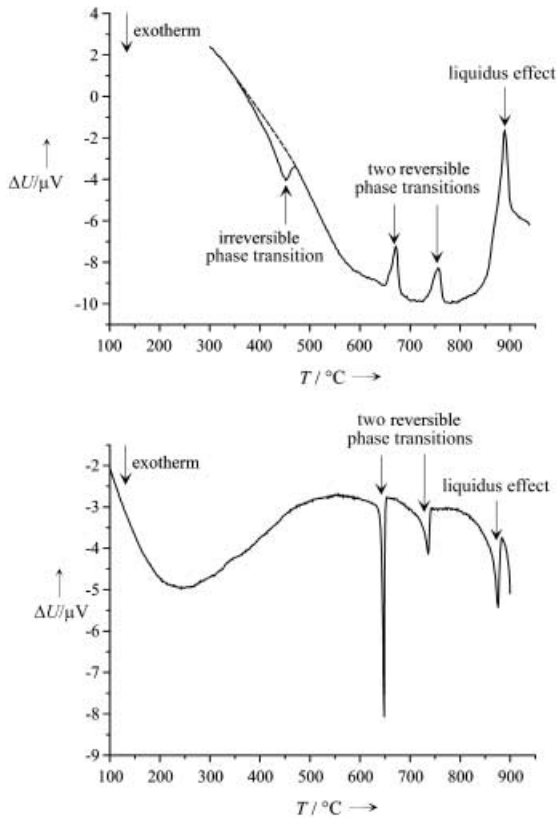

Figure 1. DTA of Rb_2Te. We used cubic, thermally untreated ω-Rb_2Te, which transformed irreversibly into orthorhombic α-Rb_2Te and then into β- and γ-Rb_2Te. Rb_2Te melts congruently at 880 °C. Top: heating curve (heating rate 5 °C min^{-1}). Under these conditions, the $\omega \rightarrow \alpha$ transition is temporarily delayed and not complete until 470 °C. Bottom: cooling curve (cooling rate 5 °C min^{-1}). There is no retransformation into the cubic phase.

Herein, the phase that is metastable at room temperature is termed the ω modification[*] and the stable phase is referred to as the α modification. A complete $\omega \rightarrow \alpha$ transformation is already observed after annealing at 350 °C for 24 h. The α modification transforms reversibly at 660 °C into β-Rb_2Te, which is transformed further into γ-Rb_2Te at 745 °C. The congruent melting point is attained at 880 °C.

Structure analysis was carried out on powder samples, and the diffraction patterns were interpreted with the aid of programs for reflection-profile analysis and Rietveld refinement (see Experimental Section). When the yellow-green product was analyzed, the diffraction patterns of the different modifications did not show any Bragg peaks of foreign phases. According to the diffraction experiments, the ω modification that is metastable at room temperature crystallizes in an anti-CaF_2-type structure with the space group $Fm\bar{3}m$ and the lattice parameter $a = 849.02(3)$ pm, isotypic to the other rubidium monochalcogenides and also to lithium-, sodium-, and potassium monochalcogenides. On the other hand, the α-Rb_2Te modification that is stable at room temperature forms the anti-$PbCl_2$-structure type with the space group *Pnma* and the lattice parameters $a = 896.60(3)$, $b = 557.15(2)$, and $c = 1095.43(3)$ pm. The α phase, however, can only be obtained

[*] Priv.-Doz. Dr. K. Stöwe, Dr. S. Appel
Anorganische und Analytische Chemie und Radiochemie, FR 8.14
Universität des Saarlandes
Postfach 15 11 50, 66041 Saarbrücken (Germany)
Fax: (+49) 681-302-4233
E-mail: k.stoewe@mx.uni-saarland.de

[**] Chemistry of rubidium telluride, Part 1. This work was supported by the Fonds der Chemischen Industrie.

[*] The authors are aware that there is no consistent system for the designation of polymorphic forms.[9]

  1433-7851/02/4115-2726 $ 20.00+.50/0

as the single-phase product when using the yellow-green product that has undergone little or no extraction with ammonia. After annealing and transformation into the modification that is stable at room temperature, the light-yellow product shows, in addition to the α-Rb_2Te Bragg peaks, further low-intensity peaks of additional phases in the diffraction pattern. These peaks can be assigned to the neighboring phase Rb_5Te_3. We can conclude from this result that the ω modification has a larger compositional width than the other modifications. Transformation into the α modification again results in a second phase with a lower Rb content than Rb_2Te. This result is reinforced by reexamination of the Rb–Te phase diagram by DTA measurements, which will be reported elsewhere. These investigations show that based on thermal effects, the light-yellow product can be ranged in a molar composition of $0.333 < x\,(\mathrm{Te}) < 0.4$.

The two observed structure types show different anion coordination environments: The Te atoms in ω-Rb_2Te with the Li_2O structure are surrounded by eight Rb atoms in the form of a cube. In α-Rb_2Te with the anti-cotunnite or $PbCl_2$ structure, nine Rb atoms surround the Te atoms in the shape of a distorted threefold-capped trigonal prism (Figure 2). This phase transition is well known in the literature; however, it is pressure- and not temperature-induced. For example, the difluorides of Ca, Cd, Sr, Eu, Ba, and Pb[10, 11] or the dioxides of Ce, Th, and Pu[12, 13] show this phase transition. It follows the pressure-coordination rule and represents the only known type of phase transition with a change in coordination number from 8 to 9.[14] In the case of Rb_2Te we can deduce by following the Ostwald rule that synthesis in liquid ammonia at first generates a metastable modification with low density, which is transformed into the denser stable modification at higher temperatures.

The structural degrees of freedom that refer to the lattice parameter relations of the orthorhombic cotunnite-structure type (space group *Pnma*) have already been analyzed and plotted in structure maps such as that shown in Figure 3.[15–17] Beck and Beyer showed that the ionic representatives of the $PbCl_2$ type can always be assigned to one of exactly three POPS-topologies (POPS = Periodic Zero Potential Surface)[18] which means that a further subdivision of the structure map is possible. By extending the structure map to the di(alkali-metal) monochalcogenides that crystallize in the anti-cotunnite type, it will become apparent that they belong to the $PbCl_2$ family and not to the SbSI family. The lower part of Figure 3 shows how α-Rb_2Te changes its position in the structure map with increasing temperature: During the thermal expansion, the point for α-Rb_2Te moves to a zone of intermetallic Co_2P-type compounds. At the temperature of the phase transition into the hexagonal modification β-Rb_2Te ($T_U = 660\,^\circ\mathrm{C}$), there are large discontinuities in the lattice parameters *b* and *c* after the transformation of the hexagonal cell into an orthorhombic setting (Figure 4, top), which is also noticeable in the structure map. The lattice parameter *a* as well as the molar volume (Figure 4, bottom) show hardly any discontinuities, which points to a relatively large displacive and only a small reconstructive character in the transformation (see discussion below on the symmetry relations between the space groups).

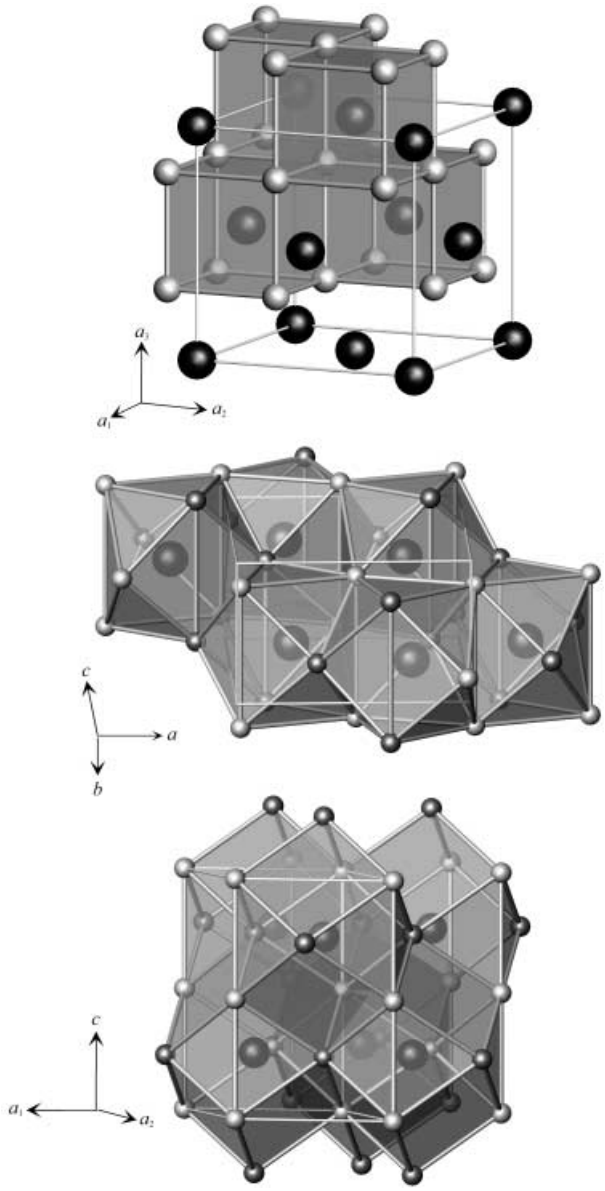

Figure 2. Crystal structures of ω-Rb_2Te (anti-CaF_2 type, top), α-Rb_2Te (anti-$PbCl_2$ type, middle), and β-Rb_2Te (Ni_2In type, bottom); Te: big, dark-gray spheres; Rb: small, light- and medium-gray spheres.

The X-ray diffraction pattern of the high-temperature phase above $T = 680\,^\circ\mathrm{C}$ can be indexed in an orthorhombic crystal system, but also in a hexagonal system. The hexagonal lattice parameter relations as well as the peak intensities indicate the Ni_2In-structure type for this modification. The space group of this type is $P6_3/mmc$ and for β-Rb_2Te the lattice parameters $a = 611.10(5)$ and $c = 919.0(1)$ pm have been refined for $T = 680\,^\circ\mathrm{C}$. The Ni_2In-structure type is a filled NiAs-type structure and features relatively high coordination numbers of the atoms. Thus Rb(1) in β-Rb_2Te is surrounded by $12 + 2$ neighbors in the form of a double-capped hexagonal prism in which the close neighbors are six Rb(2) and six Te atoms at equal distances, whereas the caps of the prism are formed by two slightly more distant Rb(1) atoms. The coordination environments of Rb(2) and Te are geometrically

  1433-7851/02/4115-2727 $ 20.00+.50/0

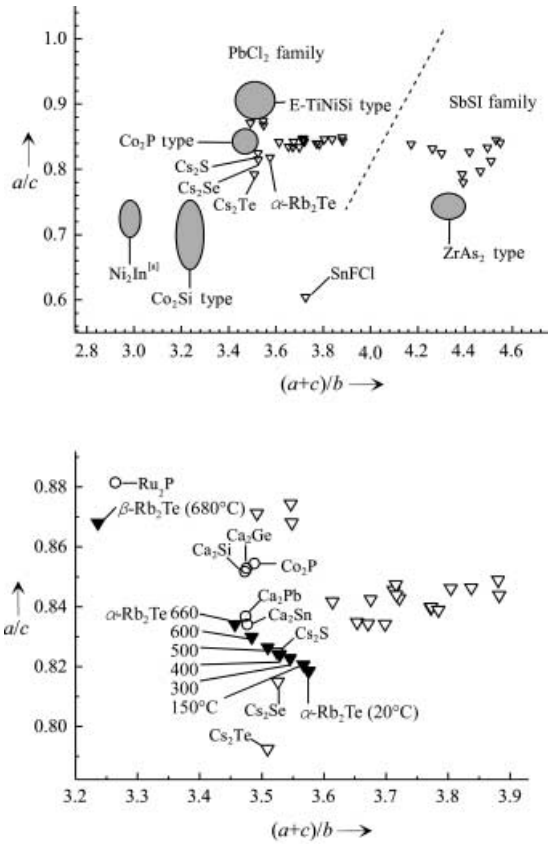

Figure 3. Extended structure map of the $PbCl_2$-type according to Jeitschko.[17] The regions of the covalent and the intermetallic compounds are marked in gray and partly scaled down. Top: overview. Bottom: detail with thermal behavior of Rb_2Te.[4, 6, 17, 18, 20, 25] [a] Ni_2In does not belong to the $PbCl_2$-structure type; however, transformed data have been added to the diagram,[26] as this crystal structure represents the aristotype of the anti-$PbCl_2$-structure type.

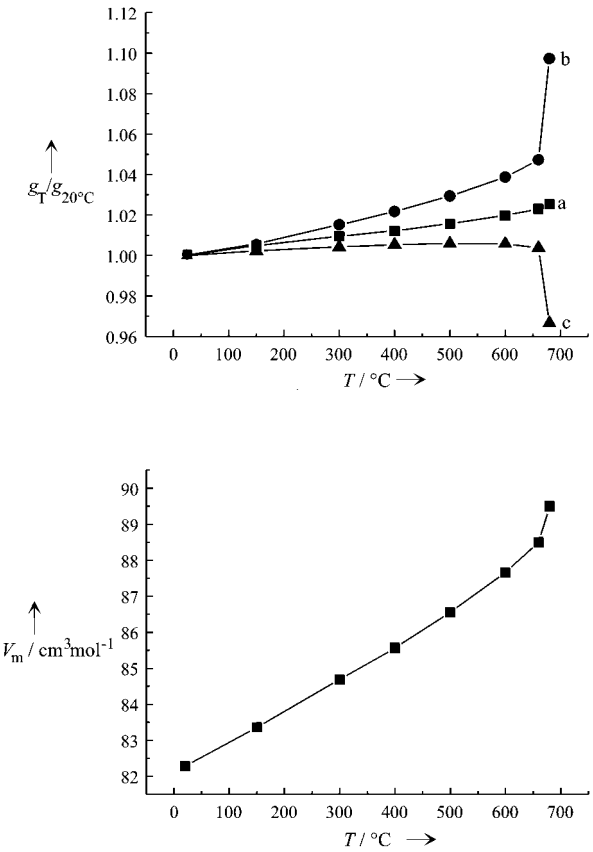

Figure 4. Anisotropic thermal expansion behavior of Rb_2Te, including the region of the $\alpha \rightarrow \beta$ phase transition (transformed parameters). Top: relative lattice parameters. Bottom: molar volume.

equal: 11 neighbors surround these atoms in form of a fivefold-capped trigonal prism. This belongs to the class of Edshammar polyhedra and is denoted ^{11}E.[19] The β-Rb_2Te structure can therefore be described as a hexagonally closest packed arrangement of Edshammar polyhedra with central Rb(2) atoms (Figure 2). This is similar to the NiAs-structure type; however, in this case all Edshammar polyhedra remain empty.

The large displacive component in the transformation of the anti-cotunnite- into the Ni_2In-structure type also becomes clear when comparing the two structure types by examining the β-Rb_2Te structure in the $[1\bar{1}0]$ direction (Figure 5). The structure relations between the two types can also be illustrated by a group–subgroup relation of the two space groups, as already described by Trübenbach[20] (Scheme 1). The space group $P6_3/mmc$ represents the supergroup, whose symmetry can be reduced to the space group of the $PbCl_2$ type in a "translationengleichen" step of index 3 and a "klassengleichen" step of index 2. The $[1\bar{1}0]$ direction of the Ni_2In type corresponds to the b axis after transformation into the orthorhombic crystal system. We thus obtain a picture of the two structures that accentuates the sheet character of the edge-sharing trigonal prisms of the Rb atoms coordinated to the Te atoms. In the Ni_2In type, these prisms are not trigonally but fivefold-capped; two further atoms are added to the coordination environment during the reduction of the folding towards planar sheets.

Based on the observations concerning the coordination numbers, we can expect that this type of phase transition can also be induced by pressure. Thus, BaF_2 not only shows the fluorite-to-cotunnite transition at $p = 3.0$ GPa, but also a second transition to the anti-Ni_2In type above 12 GPa.[21] Further examples for this high-pressure polymorphism series are the compounds Na_2Te and Na_2S: their transition pressures are $p = 2.3$ GPa and 7 GPa (fluorite-to-cotunnite type) and $p = 5.3$ GPa and 16 GPa (cotunnite-to-Ni_2In type), respectively.[22, 23] As a high-temperature variant of the $PbCl_2$ type, the Ni_2In type appears, for example, for the compound MnCoGe.[24] During the $\alpha \rightarrow \beta$ transition in Rb_2Te, besides the increase in the coordination numbers, the interatomic distances also increase, which corresponds to the pressure–distance paradox (typical for high pressure phases). At the same time, the density decreases (typical for high-temperature phases) during phase transition from $\rho_{calcd} = 3.373(1)\ g\,cm^{-3}$ at $T = 660\,^{\circ}C$ to $\rho_{calcd} = 3.336(1)\ g\,cm^{-3}$ at $T = 680\,^{\circ}C$.

The crystal structure of the fourth modification, γ-Rb_2Te, which is stable above 745 °C (second high-temperature modification), could not be determined so far. Powder-diffraction patterns have been taken at 750 to 770 °C; however

  1433-7851/02/4115-2728 $ 20.00+.50/0

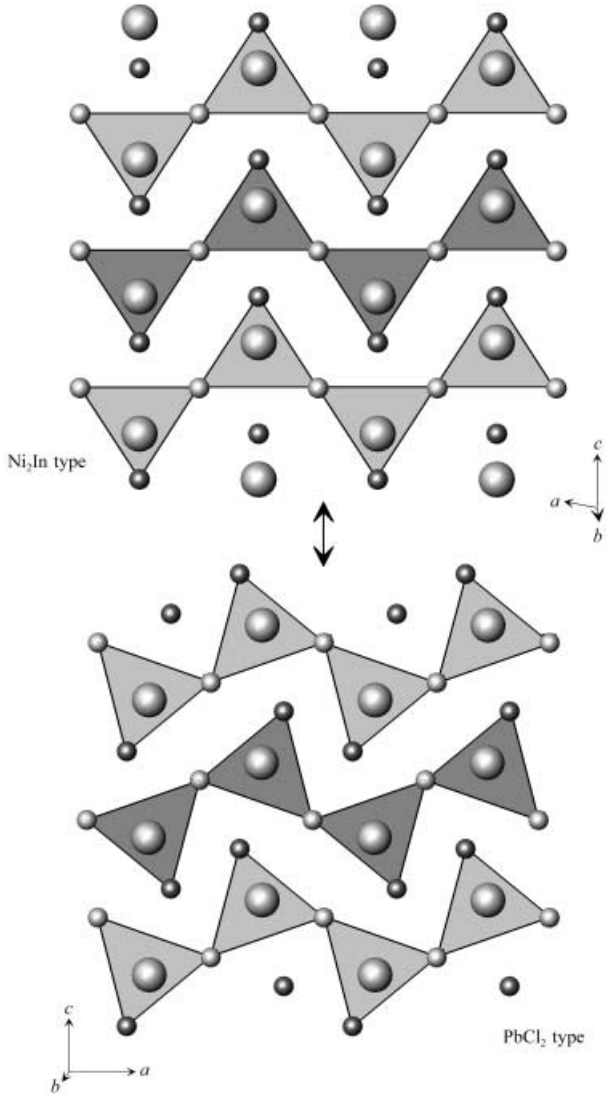

Figure 5. High-temperature-phase β-Rb_2Te (Ni_2In type) and the modification that is stable at room temperature (α-Rb_2Te, $PbCl_2$ type) with a perspective in the $[1\bar{1}0]$ direction. Te = large spheres, Rb(1) = small light-grey spheres, Rb(2) = medium grey spheres.

the quality of these measurements must be improved in the future to obtain a better signal-to-noise ratio. A problem is that at these temperatures the glass wall of the capillary is no longer inert towards the sample over extended periods of time. Furthermore, the reversible phase transition $\beta \rightarrow \gamma$ is often incomplete. Further evidence for the existence of a fourth modification of the congruent melting compound Rb_2Te is seen in the Rb–Te phase diagram, for example, corresponding two-phase regions are observed in DTA experiments.

Our studies of the compound Rb_2Te provided some very surprising results. This compound, whose structure has not been characterized for many years, is an exception within the di(alkali-metal) monochalcogenides, as it can exist in two modifications at room temperature: a metastable modification of the anti-fluorite type and a stable modification of the anti-cotunnite type. Synthesis experiments with Cs_2Te showed that the product formed during synthesis in liquid ammonia is amorphous (X-ray diffraction experiments) and transforms immediately to the anti-$PbCl_2$ type when annealed. Another unique observation is the existence of further polymorphic high-temperature phases for Rb_2Te. The structure type of one of these phases (β-Rb_2Te) has only been found among the tellurides only for Na_2Te as a high-pressure phase above $p =$ 5.3 GPa.[22] Besides the structure of the second high-temperature phase, we are currently analyzing the high-pressure polymorphic forms of Rb_2Te. Furthermore, we are working on a more specific explanation of the polymorphic relations of Rb_2Te by means of quantum-theory calculations. The results of these experiments will be discussed separately.

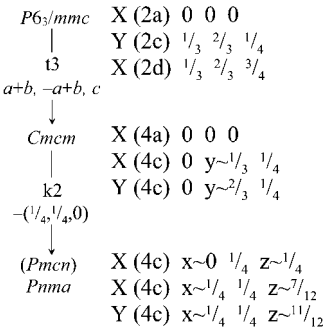

Scheme 1. Structural relation between α- and β-Rb_2Te in the form of group–subgroup relations between the space groups of the two polymeric forms.

Experimental Section

Synthesis of Rb_2Te: The synthesis of Rb_2Te was carried out in Duran laboratory glassware described in Ref. [8] from the elements (Rb from Chempur, purity 99.9%; Te from Alpha, purity 99.99999%) in liquid ammonia with a small excess of rubidium. Because rubidium as well as the product are very air-sensitive, both reagents were handled in a glovebox (Braun) in an inert Ar atmosphere. To eliminate the excess rubidium, the raw product was extracted with liquid ammonia in a special glass apparatus. The ampoules were subsequently sealed under high-vacuum conditions.

DTA: Rb_2Te was transferred into silica-glass ampoules in a glovebox and these were sealed under high-vacuum conditions. The heating and the cooling curves were plotted with a simultaneous thermal analyzer (STA409, Netzsch) with heating rates of 2–5 °C min^{-1}. The transition temperatures were taken from the heating curves by extrapolation of the peak-onset temperatures, the melting temperature by determination of the peak maximum of the liquidus effect.

X-ray characterization: All diffraction patterns were taken from powder samples filled into silica capillaries with an outer diameter of 0.2–0.3 mm and under an Ar atmosphere. To reduce the absorption coefficient, the substance was diluted with Si or silica-glass powder. The intensity measurements were carried out on an automatic four-circle diffractometer with a quartz crystal monochromator and a position-sensitive detector (OED50S, Braun) filled with an argon–methane mixture. A Seifert MZ4-type goniometer was used. The diffraction patterns were evaluated with the programs FORMFIT,[27] WIN-Rietveld,[28] and GSAS.[29] For high-temperature diffraction measurements we used a heating device on the powder diffractometer, consisting of an electrically heatable corundum fork, a Pt/Rh–Pt thermoelement, an aluminum cap, and X-ray-amorphous Kapton foil. The temperature was regulated with an electronic controller (HTC9634, Huber). The temperature regulation was calibrated up to about 700 °C by thermal dilatation of NaCl, and the temperature scale was checked by means of the phase transition of potassium chromate at 665 °C.

Structure refinement: ω-Rb_2Te: cubic, space group $Fm\bar{3}m$, $a =$ 849.02(3) pm, $V = 6.1200(6) \times 10^8$ pm^3, $\rho_{calcd} = 3.2401(3)$ g cm^{-3}, $Cu_{K\alpha 1}$ radi-

ation ($\lambda = 154.056$ pm), $T = 20\,^{\circ}$C, 21 measured reflections ($2\Theta_{max} = 94^{\circ}$, $\Delta 2\Theta = 0.01^{\circ}$), no absorption correction, refinement program: WIN-Rietveld,[28] background: linear interpolation, peak profile function: pseudo-Voigt, zero-point shift: $\Delta 2\Theta = -0.017(3)^{\circ}$, 18 refined parameters (Rb_2Te + Si), $R_p = 3.79\,\%$, $R_{wp} = 4.87\,\%$, atomic sites: Rb (8c) ¼¼¼, Te (4a) 000. α-Rb_2Te: orthorhombic, space group *Pnma*, $a = 896.60(3)$ pm, $b = 557.15(2)$ pm, $c = 1095.43(3)$ pm, $V = 5.4722(4) \times 10^8$ pm^3, $\rho_{calcd} = 3.624(1)$ g cm^{-3}, $Cu_{K\alpha 1}$ radiation ($\lambda = 154.056$ pm), $T = 20\,^{\circ}$C, 263 measured reflections ($2\Theta_{max} = 94^{\circ}$, $\Delta 2\Theta = 0.01^{\circ}$), no absorption correction, refinement program: GSAS,[29] background: Chebyshev function with 36 coefficients, peak profile function: modified Thompson – Cox – Hastings pseudo-Voigt, zero-point shift: $\Delta 2\Theta = -0.003(1)^{\circ}$; 20 refined parameters (without background), $R_p = 2.54\,\%$, $R_{wp} = 3.31\,\%$, atomic coordinates of all atoms at the site (4c) x ¼ z: $x(Rb(1)) = 0.0271(3)$, $z(Rb(1)) = 0.1784(2)$, $x(Rb(2)) = 0.1534(2)$, $z(Rb(1)) = 0.5728(2)$, $x(Te) = 0.2483(2)$, $z(Te) = 0.8860(1)$. Furthermore, diffraction patterns were taken at higher temperatures with a heating fork (Table 1), $2\Theta_{max} = 65^{\circ}$, refinement program:

Table 1. Lattice parameters, unit cell and molar volumes of α-Rb_2Te at different temperatures.

T [°C]	a [pm]	b [pm]	c [pm]	V_{EZ} [$\times 10^6$ pm^3][a]	V_{mol} [cm^3 mol^{-1}]
20	896.28(1)	556.90(1)	1094.98(3)	546.54(3)	82.282(5)
150(3)	900.70(5)	560.13(3)	1097.52(5)	553.71(9)	83.36(1)
300(3)	904.83(6)	565.37(3)	1099.65(6)	562.5(1)	84.69(1)
400(3)	907.25(6)	569.01(3)	1100.83(6)	568.3(1)	85.56(1)
500(5)	910.36(4)	573.28(1)	1101.58(3)	574.91(5)	86.553(8)
600(5)	914.02(4)	578.47(1)	1101.29(3)	582.29(5)	87.665(8)
660(5)	916.9(1)	583.23(4)	1099.21(8)	587.8(1)	88.50(2)

[a] The maximum volume deviation is $dV = V(da/a + db/b + dc/c)$.

WIN-Rietveld.[28] β-Rb_2Te: hexagonal, space group $P6_3/mmc$, $a = 611.10(5)$ pm, $c = 919.0(1)$ pm, $V = 2.9723(7) \times 10^8$ pm^3, $\rho_{calcd} = 3.336(1)$ g cm^{-3}, $Cu_{K\alpha 1}$ radiation ($\lambda = 154.056$ pm), $T = 680\,^{\circ}$C, 28 measured reflections ($2\Theta_{max} = 60^{\circ}$, $\Delta 2\Theta = 0.01^{\circ}$), no absorption correction, refinement program: GSAS,[29] background: Chebyshev function with 36 coefficients, peak profile function: modified Thompson – Cox – Hastings pseudo-Voigt, zero-point shift: $\Delta 2\Theta = -0.018(3)^{\circ}$; 12 refined parameters (without background), $R_p = 3.39\,\%$, $R_{wp} = 4.34\,\%$, atomic sites: Rb(1) (2a) 000, Rb(2) (2d) ⅓⅔¾, Te (2c) ⅓⅔¼.

Received: October 30, 2001
Revised: April 9, 2002 [Z18134]

[1] E. Zintl, A. Harder, B. Dauth, *Z. Elektrochem.* **1934**, *40*, 588.
[2] P. Touzain, M. Caillet, *Rev. Chim. Miner.* **1971**, *8*, 277.
[3] K. May, *Z. Kristallogr.* **1936**, *94*, 412.
[4] H. Sommer, R. Hoppe, *Z. Anorg. Allg. Chem.* **1977**, *429*, 118.
[5] K. R. Tsai, P. M. Harris, E. N. Lassette, *J. Phys. Chem.* **1956**, *60*, 338.
[6] I. Schewe-Miller, P. Böttcher, *Z. Kristallogr.* **1991**, *196*, 137.
[7] W. Klemm, H. Sodomann, P. Langmesser, *Z. Anorg. Allg. Chem.* 1939, *241*, 281.
[8] K. Stöwe, S. Appel-Colbus, *Z. Anorg. Allg. Chem.* **1999**, *625*, 1647.
[9] International Union of Pure and Applied Chemistry, *Nomenclature of Inorganic Chemistry*, 2nd ed., Butterworths, London, **1970**, p. 90.
[10] L. Gerward, J. Staun Olsen, S. Steenstrup, M. Malinowski, S. Asbrink, W. Waskowska, *J. Appl. Crystallogr.* **1992**, *25*, 578.
[11] D. P. Dandekar, J. C. Jamieson, *Trans. Am. Crystallogr. Assoc.* **1969**, 19.
[12] S. J. Dulcos, Y. K. Vohra, A. L. Ruoff, A. Jayaraman, G. P. Espinosa, *Phys. Rev B* **1988**, *38*, 7755.
[13] J. P. Dancausse, E. Gering, S. Heathman, U. Benedict, *High Pressure Res.* **1990**, *2*, 381.
[14] J. M. Leger, J. Haines, *Eur. J. Solid State Inorg. Chem.* **1997**, *34*, 785.
[15] C. P. Shoemaker, D. P. Shoemaker, *Acta Crystallogr.* **1965**, *18*, 900.
[16] J. Flahaut, F. Thévet, *J. Solid State Chem.* **1980**, *32*, 365.
[17] W. Jeitschko, *Acta Crystallogr. Sect. B* **1968**, *24*, 930.
[18] H. P. Beck, T. Beyer, *Z. Kristallogr.* **1997**, *212*, 565.
[19] S. Lidin, M. Sommer, T. Popp, H.-G. von Schnering, *Angew. Chem.* **1992**, *104*, 936; *Angew. Chem. Int. Ed. Engl.* **1992**, *31*, 924.
[20] P. Trübenbach, Diplomarbeit, Erlangen, **1980**.
[21] J. M. Leger, J. Haines, A. Atouf, O. Schulte, S. Hull, *Phys. Rev. B* **1995**, *52*, 13247.
[22] I. Schewe-Miller, PhD Thesis, Stuttgart, **1990**; H. J. Beister, I. M. Schewe, K. Syassen, P. Böttcher, Abstract of IUCR XV Conference, Bordeaux, **1990**.
[23] A. Vegas, A. Grzechnik, K. Syassen, I. Loa, *Acta Crystallogr. Sect. B* **2001**, *57*, 151.
[24] W. Jeitschko, *Acta Crystallogr. Sect. B* **1975**, *31*, 1187.
[25] E. Dönges, *Z. Anorg. Allg. Chem.* **1959**, *263*, 112.
[26] F. Laves, H. J. Wallbaum, *Z. Angew. Min.* **1942**, *4*, 17.
[27] R. Haberkorn, ERLRAY Program for the Interpretation of X-ray Powder-Diffraction Patterns, Dudweiler, **1998**.
[28] Siemens Analytical X-ray Systems, Sigma-C GmbH, WIN-Rietveld Version 2.54, Madison, USA, **1992 – 1997**.
[29] A. C. Larson, R. B. Von Dreele, GSAS, General Structure Analysis System, Los Alamos National Laboratory, USA, **1994**.

Irreversible Adsorption of Cellobiose, Ascorbic Acid, and Tyrosine to Hydrophobic Surfaces in Water and Their Separation by Molecular Stirring

Guangtao Li, Karl Doblhofer, and Jürgen-Hinrich Fuhrhop*

Hydrophobic nanometer clefts, which are accessible from bulk water, play a role as reactive centers of enzymes and receptors.[1] In these cavities, host molecules and substrates accumulate, the size of the cavity as well as the stereochemically arrangement of hydrogen bonds seem to play a dominant role in the specific binding of the molecules.[2] Computer modeling shows that a few water layers are immobilized on the hydrophobic membrane surfaces[3] and increasing dipolar interactions were measured.[4] With respect to the strong binding of water-soluble substrates to hydrophobic surfaces, we found out experimentally, that rigid molecules with a hydrophobic and a hydrophilic edge remained fixed in hydrophobic nanometer clefts for months and did not diffuse into the neighboring bulk water. *trans*-1,2-Dihydroxycyclo-

[*] Prof. J.-H. Fuhrhop, Dr. G. Li
Freie Universität Berlin
FB Biologie, Chemie, Pharmazie
Institut für Chemie/Organische Chemie
Takustrasse 3, 14195 Berlin (Germany)
Fax: (+49) 30-838-55589
E-mail: fuhrhop@chemie.fu-berlin.de
Dr. K. Doblhofer
Fritz-Haber-Institut der Max-Planck-Gesellschaft
Faradayweg 4 – 6, 14195 Berlin (Germany)

  1433-7851/02/4115-2730 $ 20.00+.50/0